PROTEINS: Structure, Function, and Bioinformatics 57:468–480 (2004)

Escherichia coli Adenylate Kinase Dynamics: Comparison of Elastic Network Model Modes with Mode-Coupling ^{15}N-NMR Relaxation Data

N. Alpay Temiz,[1] Eva Meirovitch,[1,2] and Ivet Bahar[1]*

[1]*Center for Computational Biology & Bioinformatics, Department of Biochemistry and Molecular Genetics, School of Medicine, University of Pittsburgh, Pittsburgh, Pennsylvania*

[2]*Faculty of Life Sciences, Bar-Ilan University, Ramat-Gan 52900, Israel*

ABSTRACT **The dynamics of adenylate kinase of *Escherichia coli* (AKeco) and its complex with the inhibitor AP_5A, are characterized by correlating the theoretical results obtained with the Gaussian Network Model (GNM) and the anisotropic network model (ANM) with the order parameters and correlation times obtained with Slowly Relaxing Local Structure (SRLS) analysis of ^{15}N-NMR relaxation data. The AMPbd and LID domains of AKeco execute in solution large amplitude motions associated with the catalytic reaction Mg^{+2}*ATP + AMP → Mg^{+2}*ADP + ADP. Two sets of correlation times and order parameters were determined by NMR/SRLS for AKeco, attributed to slow (nanoseconds) motions with correlation time $\tau_\perp$ and low order parameters, and fast (picoseconds) motions with correlation time $\tau_\parallel$ and high order parameters. The structural connotation of these patterns is examined herein by subjecting AKeco and AKeco*AP_5A to GNM analysis, which yields the dynamic spectrum in terms of slow and fast modes. The low/high NMR order parameters correlate with the slow/fast modes of the backbone elucidated with GNM. Likewise, $\tau_\parallel$ and $\tau_\perp$ are associated with fast and slow GNM modes, respectively. Catalysis-related domain motion of AMPbd and LID in AKeco, occurring *per* NMR with correlation time $\tau_\perp$, is associated with the first and second collective slow (global) GNM modes. The ANM-predicted deformations of the unliganded enzyme conform to the functional reconfiguration induced by ligand-binding, indicating the structural disposition (or potential) of the enzyme to bind its substrates. It is shown that NMR/SRLS and GNM/ANM analyses can be advantageously synthesized to provide insights into the molecular mechanisms that control biological function. Proteins 2004;57: 468–480.** © 2004 Wiley-Liss, Inc.

Key words: Gaussian network model; Slowly Relaxing Local Structure; collective modes; conformational changes

INTRODUCTION

NMR spin relaxation measurements can be translated into microdynamic parameters, thereby providing important information on protein dynamics.[1–3] The N-H bond is a particularly useful probe, relaxed predominantly by dipolar coupling of the ^{15}N nucleus to the amide proton and ^{15}N chemical shift anisotropy (CSA).[4] ^{15}N relaxation data in proteins are commonly analyzed with the model-free (MF) approach, where N-H bond dynamics is represented by two types of motions assumed to be decoupled[5–7]: the global tumbling of the protein and the local motion of the N-H bond. In the extended version of the MF approach, a slow internal motion is also included in the formalism.[7]

We recently applied the Slowly Relaxing Local Structure (SRLS) approach[8,9] to NMR spin relaxation in proteins.[10] SRLS accounts for the dynamical coupling between local and global motions within the scope of a stochastic model in which the global tumbling ($\mathbf{R^C}$), the local diffusion ($\mathbf{R^L}$), the local ordering ($\mathbf{S}$), and the magnetic interactions are represented by asymmetric tensors. The spectral density is obtained by solving a two-body (N-H bond associated with $\mathbf{R^L}$, and protein associated with $\mathbf{R^C}$) Smoluchowski equation. The mode-coupling SRLS approach can be considered the generalization of the mode-decoupling MF approach. We found that the SRLS picture of N-H bond dynamics is significantly more accurate than, and in some cases qualitatively different form, the MF picture.[10–14]

NMR spin relaxation results from an ensemble of modes of motion that determine the concerted reorientation of the N-H bond and its surroundings. Methods based on principal components analysis such as normal mode analysis (NMA),[15–17] and essential dynamics analysis (EDA),[18] have been widely used to dissect protein dynamics into its contributing modes. Molecular dynamics (MD) simulations have been used in the context of NMR spin relaxation in proteins to study local motions.[19] The recently developed isotropic Reorientational Eigenmode Dynamics

Grant sponsor: NIGMS; Grant number: 065805-01A1; Grant sponsor: Israel Science Foundation; Grant number: 520/99-16.1; Grant sponsor: Damadian Center for Magnetic Resonance Research at Bar-Ilan University, Israel.

*Correspondence to: Ivet Bahar, Center for Computational Biology and Bioinformatics, Department of Biochemistry and Molecular Genetics, School of Medicine, University of Pittsburgh, Pittsburgh, PA 15261. E-mail: bahar@pitt.edu

Received 20 November 2003; Accepted 7 May 2004

Published online 12 July 2004 in Wiley InterScience (www.interscience.wiley.com). DOI: 10.1002/prot.20226

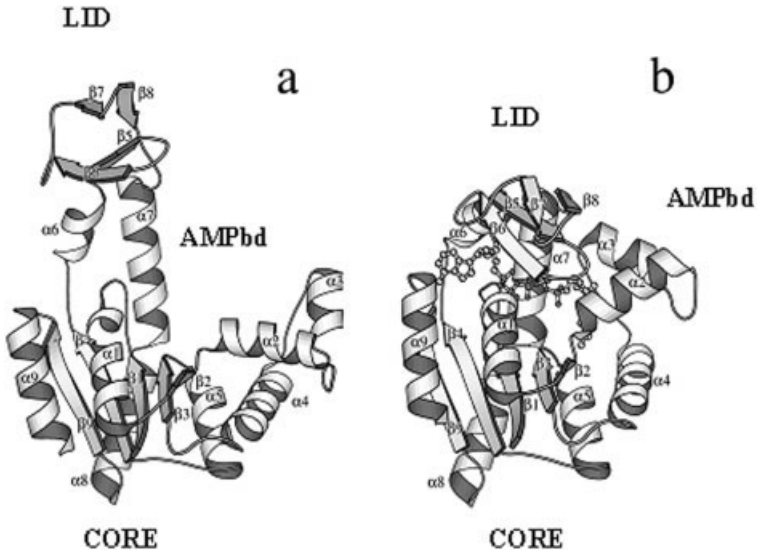

Fig. 1. Ribbon diagrams of the crystal structures of (**a**) AKeco[52] and (**b**) AKeco in complex with the two-substrate-mimic inhibitor AP_5A.[51] The figures were drawn with the program Molscript[76] using the PDB coordinate files 4ake[52] for AKeco and 1ake (complex II)[51] for AKeco*AP_5A. The AMP binding domain, AMPbd, comprises helices α_2 and α_3, the domain LID comprises the strands β_5-β_8 and the intervening loops, and the CORE domain comprises the remaining part of the polypeptide chain.

(iRED) approach[20] associates MD-based internal modes with spin relaxation data in proteins. The Gaussian network model (GNM)[21,22] and its recent extension accounting for anisotropic effects (ANM)[23] efficiently elucidate the spectrum of motions given the set of topological constraints (inter-residue contacts) in the folded state. GNM (ANM) has the advantage of yielding an analytical solution for a set of N-1 (3N-6) collective modes defined uniquely for the examined structure. In particular, the lowest frequency modes predicted by GNM/ANM, or elastic network (EN) models in general, have been shown in numerous studies[24–45] to be directly relevant to biologically functional motions.

In this study, we focus on the backbone dynamics of adenylate kinase from *Escherichia coli* (AKeco), a 23.6-kDa enzyme made of three domains: CORE, AMPbd, and LID. AKeco catalyzes the reaction Mg^{+2}*ATP + AMP → Mg^{+2}*ADP + ADP.[46,47] The CORE structure is largely preserved during catalysis whereas the domains AMPbd and LID execute large amplitude motions to configure the active site for substrate binding and disassemble it toward product release.[48–54] The structures of the ligand-free enzyme[52] and its complex with the two-substrate-mimic inhibitor AP_5A[51] are shown in Figure 1. The crystal structure of AKeco represents the "open" conformation of the enzyme [Fig. 1(a)],[52] and that of AKeco*AP_5A represents the "closed" conformation [Fig. 1(b)]. The latter was shown to be a mimic of the catalytic transition state.[55]

A substantial amount of dynamic information relevant to the solution state is currently available for AKeco and AKeco*AP_5A. The finding that the domains AMPbd and LID are engaged in large-amplitude catalysis-related displacements was first set forth by X-ray crystallographic studies.[50–52,54] Subsequently, domain motion was proven to take place *in solution* by time-resolved fluorescence energy transfer studies.[53] However, the optical studies did not provide information on motional rates, spatial restrictions implied by the segmental nature of domain motion, and the dynamic model *per se*. Toward the important goal of acquiring this information, we applied ^{15}N spin relaxation methods to AKeco and AKeco*AP_5A.[13,14,56] In our first study,[56] we used the MF approach to analyze the experimental data. Despite the fact that the experimental NOE's of AKeco were significantly depressed[14] within AMPbd and LID, which is a clear indication of slow motions, the full-fledged MF analysis yielded practically flat order parameter patterns for both enzyme forms.[56] The low performance of MF was ascribed to the neglect of mode-coupling, which is unjustified should domain motion occur on the same time scale as the global motion.[8] Within the scope of the MF analysis, we determined the global diffusion tensor using the common MF-based procedures. Although the anisotropy of the inertia tensor of the elongated crystal structure[52] [Fig.1(a)] is 1.49, the global diffusion tensor was found to be practically isotropic[56,57] with a correlation time $\tau_m = 15.1 \pm 0.1$ ns, in agreement with AKeco prevailing in solution as an ensemble-averaged structure.[13,14,53,56] This value of τ_m was confirmed by our subsequent studies.[13,14]

To test the effect of mode-coupling and local geometry, and eventually improve the analysis, we re-analyzed our data[13,14] using our recently developed SRLS approach.[10] SRLS detected very clearly domain motions in AKeco.[13] The order parameters differed significantly between the mobile domains AMPbd and LID on the one hand, and the structurally preserved domain CORE on the other hand. For the first time, the rate of domain motion in kinases was quantified and set at 8.2 ± 1.3 ns. As anticipated, this correlation time is on the order of the global motion correlation time of 15.1 ns. Hence the overall and domain

motions are necessarily coupled, explaining the significantly higher performance of mode-coupling SRLS as compared to mode-decoupled MF. Details on the MF fitting process that generated nearly the flat S^2 profiles can be found in reference[13]. SRLS also detected nanoseconds motions experienced by specific loops of AKeco*AP_5A,[14] which could be related to the dissociation of the catalytic transition state mimicked[55] by this complex.

Although the dynamic properties of AKeco and AKeco*AP_5A are thus known in considerable detail, further investigation of several key issues can be quite enlightening. For example, it would be insightful to correlate the microdynamic parameters derived with SRLS analysis with the modes computed using a different, and on some aspects complementary, physical perspective. Domain mobility renders AKeco particularly well suited to be explored with the GNM. We pursue here a combined experimental (NMR/SRLS) and theoretical (GNM/ANM) investigation of the dynamics of AKeco and its complex with AP_5A. The questions addressed are: How do the order parameters predicted by GNM correlate with those deduced from SRLS (or MF) analysis of the experimental NMR data? What is the structural connotation of the observed NMR relaxation behavior? What are the dominant mechanisms of backbone motion, and how are they reflected in the experimentally determined order parameters? What is the relation between the observed and computed low frequency (global) GNM modes and the functional motions of the enzyme?

THEORY

The Slowly Relaxing Local Structure Approach

SRLS is an effective two-body model for which a Smoluchowski equation representing the rotational diffusion of two coupled rotors is solved.[8–10] In SRLS, the coupling between the global diffusion frame (C) and local diffusion frame (M) rigidly attached to the N-H bond is accounted for by a potential $U(\Omega_{CM})$, where Ω_{CM} denotes the Euler angles between the two frames. $U(\Omega_{CM})$ can be expanded in the full basis set of Wigner rotation matrix elements, $D^L_{KM}(\Omega_{CM})$. If only the lowest order (L = 2) terms are preserved, the potential becomes

$$U(\Omega_{CM})/k_BT = -c_0^2 D^2_{00}(\Omega_{CM}) - c_2^2[D^2_{02}(\Omega_{CM}) + D^2_{0\text{-}2}(\Omega_{CM})], \quad (1)$$

where the coefficients c_0^2 and c_2^2 account for the strengths of the axial and rhombic contributions, respectively. The local ordering at the N-H bond is described by the ordering tensor, **S**, the principal values of which are the ensemble averages

$$S_0^2 = \langle D^2_{00}(\Omega_{CM})\rangle \quad (2)$$

and

$$S_2^2 = \langle D^2_{02}(\Omega_{CM}) + D^2_{0\text{-}2}(\Omega_{CM})\rangle. \quad (3)$$

Axial potentials feature only the first term of eq 1, ($S_2^2 = 0$).

In the absence of an ordering potential, the solution of the Smoluchowski equation yields three distinct eigenvalues (or correlation times τ_K; K = 0, 1, 2) for the local motion

$$(\tau_K)^{-1} = 6R^L_\perp + K^2(R^L_\parallel - R^L_\perp), \quad (4)$$

where $R^L_\parallel$ and $R^L_\perp$ are the relaxation rate constants parallel and perpendicular to the ^{15}N-^{1}H bond vector, with $R^L_\parallel = 1/(6\tau_\parallel)$ and $R^L_\perp = 1/(6\tau_\perp)$. Each K value leads to its own spectral density component $j_{K=0}(\omega)$, $j_{K=1}(\omega)$, and $j_{K=2}(\omega)$.[57,58] For magnetic tensors that are axially symmetric in the M frame, only $j_{K=0}(\omega)$ enters the measurable spectral density (defined below). Otherwise all three components $j_{K=0}(\omega)$, $j_{K=1}(\omega)$, and $j_{K=2}(\omega)$ determine the spectral density. When the potential $U(\Omega_{CM})$ is infinitely strong, and if the protein is approximated by a spherical top, then the measurable spectral density reduces to $\tau_m/(1 + \omega^2\tau_m^2)$ where $\tau_m = (6R^C)^{-1}$ is the correlation time for overall tumbling and R^C is the isotropic diffusion rate.

In the general case, the solution consists of multiple modes, (j), expressed in terms of the eigenvalues $1/\tau(j)$ and weighing factors $c_i(j)$ such that[8–10]

$$j_K(\omega) = \sum_j c_K(j)\tau(j)/(1 + \omega^2(\tau(j))^2). \quad (5)$$

The eigenvalues $1/\tau(j)$ refer to pure or mixed dynamic modes, in accordance with the parameter range considered. Concise expressions for the SRLS spectral density for dipolar auto-correlation, $J^{dd}(\omega)$, ^{15}N CSA auto-correlation, $J^{cc}(\omega)$, and ^{15}N CSA – ^{15}N-^{1}H dipolar cross-correlation, $J^{cd}(\omega)$, are

$$J^x(\omega) = A(x)j_{K=0}(\omega) + B(x)j_{K=1}(\omega) + C(x)j_{K=2}(\omega), \quad (6)$$

where the coefficients A(x), B(x), and C(x), with x denoting cc, dd, or cd, feature the trigonometric expressions obtained by the frame transformations.[8,9,57,58] The measurable spectral densities are calculated as a function of $J(0)$, $J(\omega_N)$, $J(\omega_H)$, $J(\omega_H + \omega_N)$ and $J(\omega_H - \omega_N)$ (obtained from $J^x(\omega)$ by including the magnetic interactions) using standard expressions for NMR spin relaxation.[4,59] Details on the implementation of SRLS in a data-fitting scheme featuring axial potentials were outlined previously.[10]

The Model-Free Approach.

In the MF approach[5–7], the overall tumbling of the protein and an effective local N-H motion are assumed to be decoupled. Consequently, the correlation function for N-H bond motion is the product of the correlation functions corresponding to these two types of motions, i.e.,

$$C(t) = C^C(t)C^L(t), \quad (7)$$

Here $C^C(t) = 1/5\exp(-t/\tau_m)$ is the correlation function for isotropic overall tumbling and $C^L(t)$ is the correlation function for local motions, expressed as $C^L(t) = S^2 + (1 - S^2)\exp(-t/\tau_e)$,[5,6] where τ_e denotes the effective local motion correlation time, and S^2 is the squared generalized order parameter defined as $S^2 = C^L(\infty)$. Mode-decoupling is implied by $\tau_e \ll \tau_m$. The measurable spectral density, $J(\omega)$, is given by[5,6]

$$J(\omega) = j_{K=0}(\omega) = S^2[\tau_m/(1 + \omega^2\tau_m^2)] + (1 - S^2)[\tau_{eff}/(1 + \omega^2\tau_{eff}^2)], \quad (8)$$

where $\tau_{eff}^{-1} = \tau_m^{-1} + \tau_e^{-1}$. If the equilibrium distribution of N-H orientations is axially symmetric, then $S^2 = \langle[3/2\cos^2\beta_{CM} - \frac{1}{2}]\rangle^2$ where β_{MC} is defined by $\Omega_{MC} = (0, \beta_{MC}, 0)$. When eq 8 cannot fit the experimental data, the extended MF spectral density[7]

$$J(\omega) = S_f^2\{S_s^2\tau_m/(1 + \omega^2\tau_m^2) + [1 - S_s^2]\tau_s'(1 + \omega^2\tau_s'^2)\} + [1 - S_f^2]\tau_f'(1 + \omega^2\tau_f'^2) \quad (9)$$

is used, where $1/\tau_f' \equiv 1/\tau_f + 1/\tau_m$ and $1/\tau_s' \equiv 1/\tau_s + 1/\tau_m$, τ_f is the correlation time for a fast internal motion associated with a squared generalized order parameter S_f^2, and τ_s the correlation time for a slow internal motion associated with a squared generalized order parameter, S_s^2. The slow internal motion occurs on the same time scale as the global tumbling whereas τ_f is much shorter.

The Gaussian Network Model

In the GNM, the protein is viewed as an elastic network, the nodes of which are the amino acids represented by their C^α atoms. All residue pairs located within a cutoff distance of r_c are assumed to be coupled (or connected) via a harmonic potential (or a spring) with a uniform force constant (γ), which stabilizes the native structure.[21,25] The equilibrium correlation $\langle \Delta\mathbf{R}_i \cdot \Delta\mathbf{R}_k \rangle$ between the fluctuations $\Delta\mathbf{R}_i$ and $\Delta\mathbf{R}_k$ of the α-carbons i and k is given by

$$\langle \Delta\mathbf{R}_i \cdot \Delta\mathbf{R}_k \rangle = (k_B T/\gamma)[\mathbf{\Gamma}^{-1}]_{ik}, \quad (10)$$

where k_B is the Boltzmann constant, T the absolute temperature, $\mathbf{\Gamma}^{-1}$ the inverse of Kirchhoff matrix of contacts characteristic of the examined structure, and the subscript ik denotes the ikth element of the matrix. The off-diagonal elements of $\mathbf{\Gamma}$ are given by $\mathbf{\Gamma}_{ij} = -1$ if residues i and j are connected, and are zero otherwise. The diagonal elements of $\mathbf{\Gamma}$ are found from the negative sum of the elements in the corresponding column (or row), such that $\mathbf{\Gamma}_{ij}$ is equal to the number of inter-residue contacts that the ith residue makes.[21,25] A cutoff distance r_c = 10 Å is adopted here, which is long enough to include all bonded and non-bonded neighbors within a first coordination shell.[60]

A major attribute of the GNM is its ability to assess the contribution of individual modes to the observed dynamics. The cross-correlation $\langle \Delta\mathbf{R}_i \cdot \Delta\mathbf{R}_k \rangle$ may be expressed as a sum over N-1 collective modes found from the eigenvalue decomposition of $\mathbf{\Gamma}$, ranging from fast and localized motions to slow and highly cooperative motions, i.e.,

$$\langle \Delta\mathbf{R}_i \cdot \Delta\mathbf{R}_k \rangle = (3k_B T/\gamma)[\Sigma\lambda_j^{-1}\mathbf{u}_j\mathbf{u}_j^T]_{ik} = (3k_B T/\gamma)\Sigma A_{ik}^{(j)} \quad (11)$$

Here λ_j is the jth eigenvalue of $\mathbf{\Gamma}$, $\mathbf{u}_j$ is the jth eigenvector, and $A_{ik}^{(j)} = [\lambda_j^{-1}\mathbf{u}_j\mathbf{u}_j^T]_{ik}$ represents the contribution of the jth mode to $\langle \Delta\mathbf{R}_i \cdot \Delta\mathbf{R}_k \rangle$. Equation 11 reduces to the autocorrelation or mean-square fluctuation $\langle(\Delta R_i)^2\rangle$ when k = i.

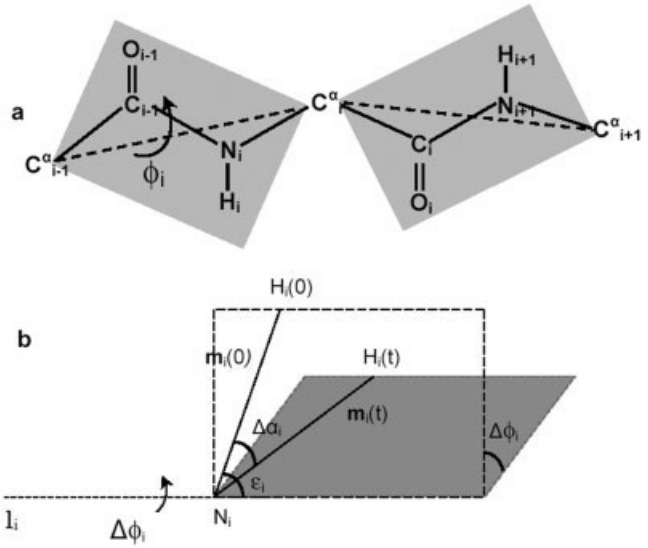

Fig. 2. **a:** Schematic of the virtual bond of the GNM theory. The chain is made of consecutive peptide planes comprising the atoms C^α_{i-1}, C'_{i-1}, N_i, and C^α_i. The bond vector N_i-H_i makes an angle ϵ_i with the virtual bond, $\mathbf{l}_i$, that connects the atoms C^α_{i-1} and C^α_i . **b:** Diagram showing the angular change $\Delta\alpha_i$ in the orientation $\mathbf{m}_i(t)$ of the bond N_i-H_i, induced by the torsional rotation, $\Delta\phi_i$, undergone by the virtual bond, $\mathbf{l}_i$. $\Delta\alpha_i$ and $\Delta\phi_i$ are related by eq 14, assuming that the angle ϵ between $\mathbf{l}_i$ and $\mathbf{m}_i(t)$ is fixed.

The GNM theory permits us to evaluate the *profile* of the residue-specific correlation times, $\tau_{i,GNM}$, for each residue i. $\tau_{i,GNM}$ scales as[22]

$$\tau_{i,GNM} \sim \langle(\Delta R_i)^2\rangle^{-1} \sum_{k=2}^{n} \frac{A_{ii}^{(k)}}{\lambda_k} \quad (12)$$

which enables us to determine the relative contribution of the individual modes. Equation 12 yields the relative values of the correlation times of individual residues, rather than their absolute values.

Calculation of Squared Order Parameters Using GNM

The local geometry near the i_{th} N-H bond is depicted in Figure 2. Figure 2(a) shows the virtual bond representation of the protein backbone. The structure is represented by a sequence of rigid planes defined by the *trans* peptide bond and the two flanking backbone bonds. The ith N-H bond lies within the peptide plane that contains the atoms C^α_{i-1}, $(C')_{i-1}$, $(N)_i$, and C^α_i. $\mathbf{l}_i$ is the virtual bond C^α_{i-1}-C^α_i about which the torsional fluctuation $\Delta\phi_i$ occurs. As shown in Figure 2(b), the bond $(N\text{-}H)_i$ makes an angle ϵ_i with $\mathbf{l}_i$. The angular change, $\Delta\alpha_i$, in the orientation of the bond $(N\text{-}H)_i$ from its original position $\mathbf{m}(0)$ to the position $\mathbf{m}(t)$ at time t is determined by the change in the virtual bond dihedral angle, ϕ_i, provided all the other bond lengths and bond angles are kept fixed. The largest contribution to $\Delta\alpha_i$ comes from the rotation $\Delta\phi_i$ of the ith virtual bond, with the effect of virtual bond rotations, $\Delta\phi_j$, decreasing with increasing separation between i and j.

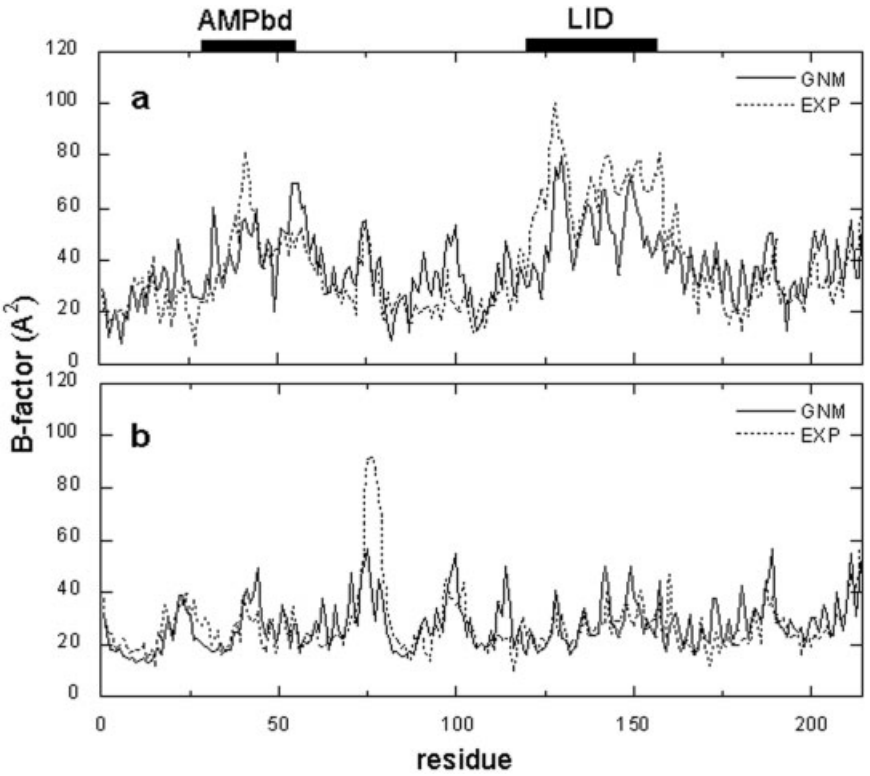

Fig. 3. Experimental[51,52] (---) and GNM-predicted (—) B-factors for AKeco (**a**) and AKeco*AP$_5$A (**b**).

In the absence of coupling between adjacent bond rotations, the GNM order parameter $S^2_{i\,GNM}$ for $(N\text{-}H)_i$ is fully determined by $\Delta\phi_i$ and given by[61]

$$S^2_{i\,GNM} = S^2(\Delta\phi_i) = 3/2\langle\cos^2\Delta\alpha_i\rangle\phi_i - \frac{1}{2} \qquad (13)$$

with

$$\langle\cos^2\Delta\alpha_i\rangle\phi_i \approx (1 - \sin^2\varepsilon) + \sin^4\varepsilon(1 - \langle\Delta\phi_i^2\rangle + 5/12\langle\Delta\phi_i^2\rangle^2) \qquad (14)$$

using the equality $\langle\cos\Delta\phi_i\rangle = 0$, and the Gaussian approximation $\langle\Delta\phi_i^4\rangle \approx (5/3)\langle\Delta\phi_i^2\rangle^2$ for small fluctuations. The problem of evaluating $S^2_{i\,GNM}$ thus reduces to determining the autocorrelation $\langle\Delta\phi_i^2\rangle$ given by

$$\langle\Delta\phi_i^2\rangle = (\mathbf{a}^T_{i+1,i}\mathbf{a}_{i+1,i})^{-1}\langle\Delta\mathbf{R}_{i+1}\cdot\Delta\mathbf{R}_{i+1}\rangle \qquad (15)$$

Here $\mathbf{a}_{ij}$ is the transformation vector that operates on the dihedral angles and transforms them into position vectors, according to the relationship $\Delta\mathbf{R}_i = \sum_{j=3}^{i-1} a_{ij}\Delta\phi_j$.[62]

Neighboring dihedral angles are interdependent due to chain connectivity and the need to localize the translational motions of the backbone. In particular, bonds i and i±2 are strongly correlated and undergo coupled counter rotations.[62–64] These couplings are accounted for by correcting eq 13 as

$$S^2_{i\,GNM} = S^2(\Delta\phi_i)[1 - \Sigma_k\Delta S^2(\Delta\phi_i, \Delta\phi_k)] \qquad (16)$$

where $\Delta S^2(\Delta\phi_i,\Delta\phi_k)$ is the contribution of $\Delta\phi_k$ to the reorientation of $(N\text{-}H)_i$ defined as

$$\Delta S^2(\Delta\phi_i, \Delta\phi_k) = [1 - S^2(\Delta\phi_k)]|\langle\Delta\phi_i\Delta\phi_k\rangle|/2 \qquad (17)$$

The cross-correlation $\langle\Delta\phi_i\Delta\phi_k\rangle$ is given by

$$\langle\Delta\phi_i\Delta\phi_k\rangle = (\mathbf{a}^T_{i+1,i}\mathbf{a}_{k+1,k})^{-1}\langle\Delta\mathbf{R}_{i+1}\cdot\Delta\mathbf{R}_{k+1}\rangle \qquad (18)$$

In the present calculations, cross-correlations up to second neighboring bonds ($|k - i| \leq 2$, $k \neq i$) were included. The contributions of the bonds k= i±1 and k = i±2 to the order parameter of $(N\text{-}H)_i$ depend on the size of the cross-correlations $\langle\Delta\phi_i\Delta\phi_k\rangle$, hence the use of the scaling term $|\langle\Delta\phi_i\Delta\phi_k\rangle|$ in eq 17. We note that equation 17 vanishes, and $S^2_{i\,GNM}$ reduces to $S^2(\Delta\phi_i)$, in the case of uncorrelated torsions, i.e., when $\langle\Delta\phi_i\Delta\phi_k\rangle = 0$. The factor $\frac{1}{2}$ in eq 17 accounts for the equal distribution of the effect of bond rotation on both sides of the rotating bond. Our previous work showed that correlations up to the second neighbors have a significant effect on $S^2_{i\,GNM}$.[61]

RESULTS AND DISCUSSION

Comparison of X-Ray Crystallographic and GNM B Factors

X-ray crystallographic temperature factors provide a measure for the mobilities of individual residues in folded protein structures. Figures 3(a) and (b) show the B-factors predicted by GNM (solid curve) superimposed on the crystallographic B-factors (dashed curve) for the ligand-free[52] and inhibitor-bound[51] forms of AKeco, respectively.

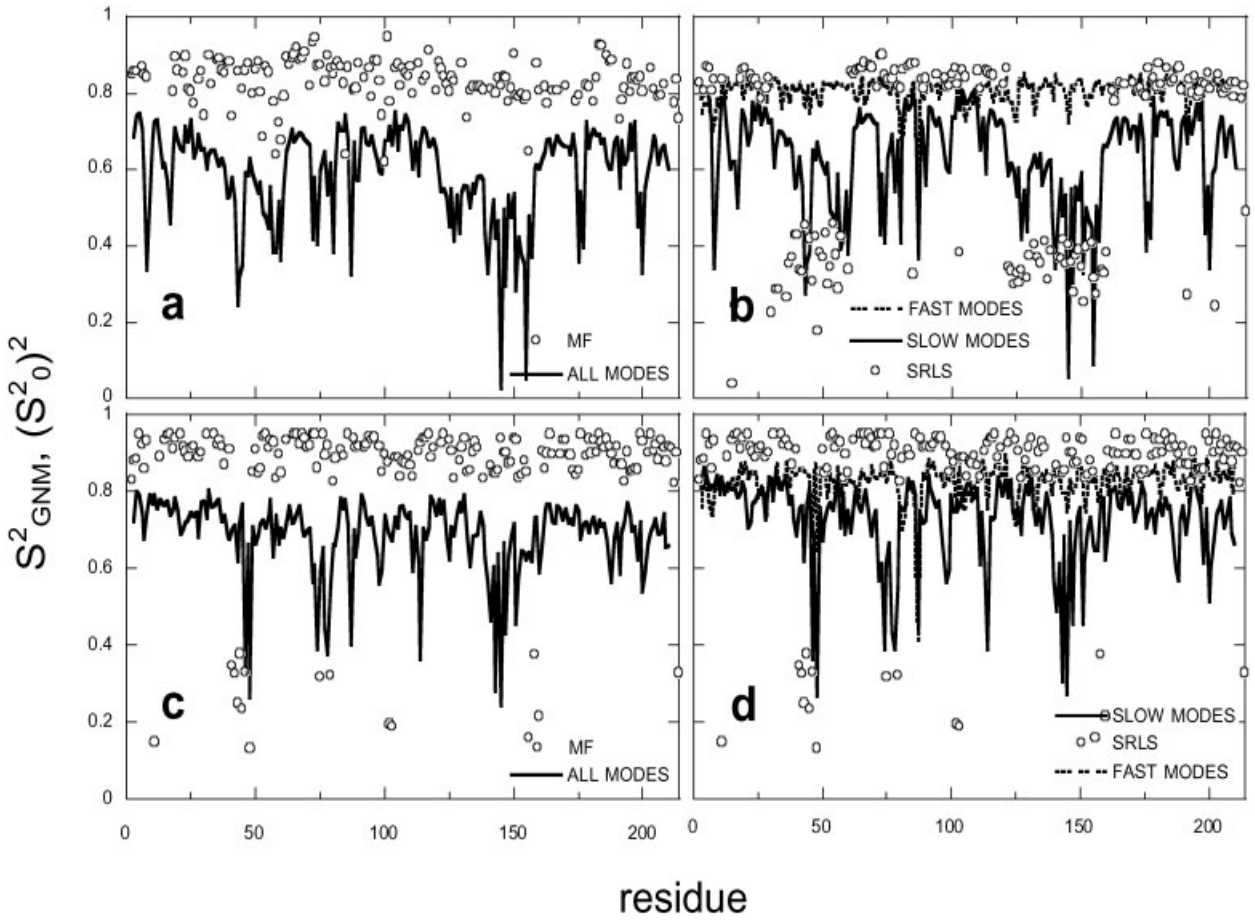

Fig. 4. **a:** NMR order parameters obtained with MF analysis (open circles)[56] and theoretical GNM order parameters (solid curve), as a function of residue number for AKeco. **b:** NMR order parameters obtained with SRLS analysis (open circles)[13] and theoretical GNM order parameters calculated from the slowest N/4 modes (solid curve) and the N/4 fastest modes (dashed curve) as a function of residue number for AKeco. **c:** Counterpart of Figure a for AKeco*AP_5A with the NMR/MF data from reference 56. **d:** Counterpart of b for AKeco*AP_5A with the NMR/SRLS data from reference 14. $(S^2_0)^2$ and S^2 were obtained by fitting the experimental ^{15}N T_1, T_2, and ^{15}N-^{11} NOE data of the two enzyme forms obtained at 303K and at 14.1/18.8 T with SRLS[13,14] and MF,[56] respectively, using τ_m = 15.1 ns for AKeco and τ_m = 11.6 ns for AKeco*AP_5A.[13]

The resolution of the crystal structure of the unliganded form is 2.2 Å with an R-value of 0.183 (PDB code: 4ake).[52] The resolution for the inhibitor bound structure is 1.9 Å with an R-value of 0.196 (PDB code: 1ake).[51] GNM force constants γ of 0.127 and 0.133 kcal/(mol.Å^2), derived from the comparison of the predicted values with experimental data, were used for AKeco and AKeco*AP_5A, respectively. γ rescales uniformly the magnitudes of the GNM B-factors for a given protein without affecting the relative residue-specific B-factors of residues or their fluctuation profiles in different modes.

The correlation coefficient between experimental and theoretical results is 0.72 for AKeco [Fig. 3(a)] and 0.59 for AKeco*AP_5A [Fig. 3(b)]. The boxes along the upper abscissa depict the domains AMPbd and LID. The high B-factors within the AMPbd and LID domains of the ligand-free enzyme point out high mobility [Fig. 3(a)]. This property was detected in previous crystallographic studies[52] as well as spectroscopic studies in solution.[13,14,53,56] Theory and experiment agree for AKeco*AP_5A as well, except for the loop α_4/β_3 (residues Q74-G80), where the crystallographic data[51] show higher mobility [Fig. 3(b)]. This loop features the sequence AQEDCRNG,[51] which includes quite a few long side chains. The enhanced mobility of such long side chains may be overlooked by the GNM.[25] Comparison of the results for AKeco [Fig. 3(a)] and AKeco*AP_5A [Fig. 3(b)] reveal the significant decrease in the mobility of the AMPbd and LID domains upon inhibitor binding.

Comparison of NMR/SRLS and GNM Squared Order Parameters

Figure 4 compares the NMR-derived (open circles) and GNM-derived (curves) squared order parameters for AKeco [Fig. 4(a,b)], and AKeco*AP_5A [Fig. 4(c,d)]. The NMR-derived $(S^2_0)^2$ values in Figure 4(a,c) were obtained previously[56] by fitting with MF the experimental data acquired at 303K, and 14.1/18.8 T, with τ_m = 15.1 ns. The corresponding $S^2_{i\,GNM}$ values were computed from the superposition of all the N-1 GNM modes (solid curves). We note that the GNM results provide information on the *distribution* of order parameters rather than their absolute values. The

correlation coefficient is in this case a good measure for comparison with the NMR data. We calculated the correlation coefficient between the two sets of data in Figure 4(a), taking running averages over three consecutive residues to minimize the noise, which yielded a correlation coefficient of 0.37. Thus, little correlation is observed even qualitatively between the theoretical GNM results and the results of the MF analysis. Moreover, Figure 4(a) shows that the known[14,52,53] mobility of the domains AMPbd and LID is practically undetected with the MF analysis, which generated a nearly flat order parameter profile, while it is detected conspicuously with the simple predictive GNM analysis by significantly depressed $S^2_{i\,GNM}$ values within AMPbd and LID.

The $(S^2_0)^2$ SRLS values (open circles) obtained[13,14] by fitting with SRLS the same experimental data as used in the MF analysis[56] are shown for AKeco in Figure 4(b) and AKeco*AP_5A in Figure 4(d). The GNM order parameters obtained form the N/4 slowest modes (solid curve), and the N/4 fastest modes (dashed curve) are shown separately. The $S^2_{i\,GNM}$ order parameters profile obtained using the complete set of N-1 modes [shown in Fig. 4(a,c)] is very similar to that obtained from the N/4 slowest modes, apart from a general decrease due to the disorder contributed by the fast modes. This close similarity emphasizes the dominant role of the slow modes. The correlation coefficient between $(S^2_0)^2$ SRLS of Figure 4(b) and all-mode $S^2_{i\,GNM}$ data is 0.65, which is a significant improvement over 0.37 obtained with the Figure 4(a) data. We note that this correlation coefficient is comparable to those recently obtained by Zhang and Bruschweiler[65] for a series of other proteins. The results in that study were found using a simple empirical expression based on the contacts made by the N-H hydrogen atom and the preceding carbonyl oxygen with heavy atoms. While this empirical expression was successful in reproducing a set of experimental data (for other proteins), physical insights on the origin and mechanisms of the molecular motions and correlations that give rise to the observed relaxation are provided by the GNM, as will be further elaborated below.

Comparison of the $(S^2_0)^2$ SRLS and $S^2_{i\,GNM}$ profiles is more meaningful than the magnitude of the empirical correlation factor. The $(S^2_0)^2$ SRLS profile shown in Figure 4(b) (open circles) singles out unequivocally the mobile domains AMPbd and LID. Except for a few outliers within CORE, low $(S^2_0)^2$ values on the order of 0.35 are encountered exclusively within AMPbd and LID, whereas much higher values, on average 0.86, are encountered within CORE. Inasmuch as GNM predicts the *relative* values, it is meaningful to examine the ratio of the computed squared order parameters at the rigid (CORE) and the mobile (AMPBd and LID) domains. An average $S^2_{i\,GNM}$ value of 0.69 is found from the slow modes for CORE while AMPbd and LID exhibit $S^2_{i\,GNM}$ values as low as 0.35–0.40, which leads to a ratio of about 0.69:0.40. This ratio is smaller than that (0.86:0.35) indicated by the SRLS analysis. Interestingly, the high $(S^2_0)^2$ values of CORE are reproduced by considering the N/4 fastest modes exclusively (dashed curve). The superposition of the remaining $\frac{3}{4}$N GNM modes depresses the order parameters within AMPbd and LID to significantly lower values, consistent with the involvement of these domains in the slow modes.

There are several regions of the AKeco backbone that show high mobility according to $S^2_{i\,GNM}$. These include residues G7-P9 of the P-loop, residues Q16-Q18 of helix α_1, the loop α_4/β_3, residues T175-P177 linking helices α_7 and α_8, residues G144 and R156 of LID, and residues G198-P201 of the loop β_9/α_9. The N-terminal chain segment comprising the first 30 residues, which includes the P-loop and residues Q16-Q18, has been identified as a major structural block required for the stability of the native state.[66] This chain segment also plays a functional role through the P-loop binding motif. Residues T175-P177 comprise the joint IV,[51] which plays a key role in the catalysis-related movements of LID.[49]

On the whole, the $(S^2_0)^2$ SRLS and $S^2_{i\,GNM}$ profiles of AKeco agree, with extra flexibility predicted by GNM at specific chain positions within CORE, as outlined above. Perfect agreement between SRLS and GNM across the board is not to be expected. The basic tenets of these methods are different. SRLS solves the stochastic rotational diffusion equation for every N-H site in the protein.[10] GNM is based on topological considerations related to the alpha carbons.[21,22] Despite this, the simple predictive GNM method clearly detects catalysis-related domain motion in AKeco, in agreement with the SRLS analysis. As pointed out above, domain motion was proven to occur in *solution* by optical studies[53] and NMR/SRLS.[10,14] The GNM order parameters [solid curve in Figure 4(a)] concur with these results whereas the MF order parameters [open circles in Figure 4(a)] do not.

$(S^2_0)^2$ values obtained previously[14] by fitting with SRLS the experimental data obtained at 303K, 14.1/18.8T, with τ_m = 11.6 ns[13] are shown in Figure 4(d) for AKeco*AP_5A, along with the $S^2_{i\,GNM}$ curves calculated for the slowest N/4 modes (solid curve), and the fastest N/4 modes (dashed curve). The noise in the two sets of data precludes comparison in terms of a correlation coefficient. However, the fact that domain motion is discontinued upon inhibitor binding is borne out by both the $(S^2_0)^2$ and $S^2_{i\,GNM}$ profiles. The AKeco*AP_5A backbone was shown in previous work[14] to be quite rigid in solution, as shown by the high $(S^2_0)^2$ values. Only selected residues within the loops α_2/α_3, α_4/β_3, and α_5/β_4, and the C-terminal segment of domain LID, are flexible according to SRLS [Fig. 4(d)]. The loops α_2/α_3 and α_4/β_3 show some mobility according to both GNM and SRLS. GNM indicates mobility in the LID domain, and at several additional positions along the chain. Excluding the flexible residues mentioned above, the average $S^2_{i\,GNM}$ value obtained from the N/4 slowest GNM modes is 0.74 for AKeco*AP_5A, and the average $(S^2_0)^2$ value is 0.93. The agreement improves if the fastest N/4 modes are used to calculate $S^2_{i\,GNM}$, but it is not as good as the GNM-SRLS agreement obtained for the CORE domain of AKeco. We recently found that unduly high $(S^2_0)^2$ values may arise from using axial potential to fit the data, while the actual potentials are asymmetric.[11] For practical reasons, the $(S^2_0)^2$ values in Figure 4(d) were obtained using axial

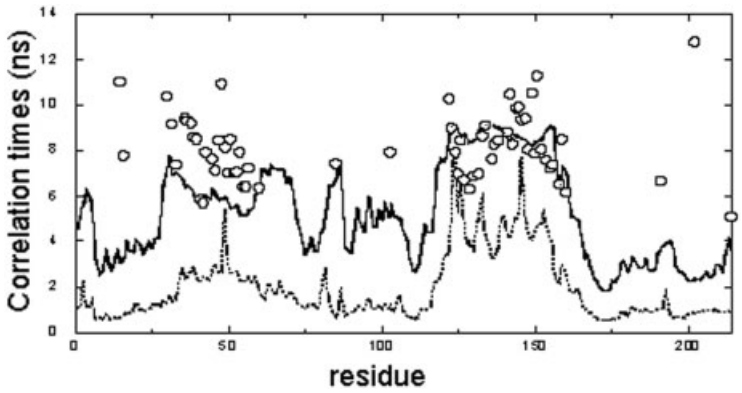

Fig. 5. Best-fit local motion correlation time component, $\tau_\perp$, obtained by fitting the experimental ^{15}N T_1, T_2, and ^{15}N-^{11} NOE data of AKeco obtained at 303K, and at 14.1/18.8 T (open circles).[13] GNM correlation times τ_{iGNM} (eq 12) obtained for AKeco from the five slowest modes (solid curve) and all the modes (dashed curve). The abscissa represents residue number.

potentials. This also applies to the AKeco $(S_0^2)^2$ values shown in Figure 4(b) but for AKeco the effect of potential asymmetry is apparently smaller.[11] A fitting scheme for SRLS allowing for asymmetric potentials, the development of which is underway, is expected to yield lower $(S_0^2)^2$ order parameters for AKeco*AP_5A in better agreement with their GNM counterparts.[11]

$S^2_{i\,GNM}$ Versus GNM B-Factors

Some chain segments are singled out as flexible by $S^2_{i\,GNM}$ (Fig. 4) but not by the B factors (Fig. 3). This behavior is rooted in the compositions of these variables. The B-factors depend on the $\langle \Delta R_i^2 \rangle$ values associated with α-carbons.[22,25,67] $S^2_{i\,GNM}$ depends on the rotational autocorrelations, $\langle \Delta\phi_i^2 \rangle$, and cross-correlations, $\langle \Delta\phi_i \Delta\phi_k \rangle$, derived from $\langle \Delta\mathbf{R}_i \cdot \Delta\mathbf{R}_k \rangle$.[61] Translational and orientational fluctuations are usually correlated, but need not be identical.[25] $S^2_{i\,GNM}$ provides a measure for the rotational mobility of the backbone, which may in some cases tend to localize the translational motions of the backbone. The loop α_2/α_3 (residues S44-Q48) of AKeco*AP_5A is a typical example shown by both $(S_0^2)^2$ and $S^2_{i\,GNM}$ to experience high rotational mobility [Fig. 4(d)], but confined to relatively restricted spatial displacements according to crystallographic and GNM-derived B-factors [Fig. 3(b)]. This chain segment is part of the α_2 helix in AKeco and represents a loop in AKeco*AP_5A, constituting the only secondary structure element which is altered upon AP_5A binding.[52]

NMR/SRLS and GNM Correlation Times

The SRLS squared order parameters of AKeco are clustered into two distinct ranges as can be clearly seen in Figure 4(b).[13] High order parameters have been associated with "ps regime" dynamics (correlation times $\tau_\parallel$ on the order of picoseconds) and low order parameters with "ns regime" dynamics (correlation times $\tau_\perp$ on the order of nanoseconds, and $\tau_\parallel \ll \tau_\perp$).[10,13,14] Comparison with GNM results lends support to the association of low NMR/SRLS order parameters with slow GNM modes and high NMR/SRLS order parameters with fast GNM modes. It is of interest to find out whether $\tau_\perp$ and $\tau_\parallel$ may similarly be associated with the correlation times corresponding to the GNM slow and fast modes, respectively.

The GNM correlation times calculated for AKeco using eq 12 are shown in Figure 5 (solid and dashed curves). The open circles are the NMR/SRLS $\tau_\perp$ values previously calculated, which appear predominantly within AMPbd and LID.[13] The $\tau_{i,GNM}$ values are found from the five slowest GNM modes, with a proportionality constant of $\tau_0 = 2.5$ ns. These modes (solid curve) make a fractional contribution of $\Sigma_{k=1}^{5} \lambda_k^{-1} / \Sigma_{k=1}^{N-1} \lambda_k^{-1} = 0.3$ to the observed dynamics. The proportionality constant $\tau_0 = 2.5$ ns rendered these data comparable in magnitude to $\tau_\perp$. The dashed curve shows τ_{iGNM} values computed from the superposition of *all* the GNM modes. The correlation times corresponding to slower modes (solid curve) are longer than those resulting from "all" modes, because of the contribution of a larger number of modes to relaxation in the "all-modes" scenario. The τ_{iGNM} profile based on the five slowest modes shows broad peaks at the AMPbd and LID domains. This suggests that the SRLS $\tau_\perp$ values that represent the correlation time for domain motion[13] can be associated with the GNM slow modes.

The previous NMR/SRLS analysis set $\tau_\parallel$ in the range of 7–200 ps.[13] The fastest N/4 modes (not shown) yielded an average correlation time of 115 ps with a relatively uniform distribution over the chain (similar to the fast-mode-based $S^2_{i\,GNM}$ values) [dashed curve in Fig. 4(b)], in agreement with the median $\tau_\parallel$ value. This indicates that it is possible to associate $\tau_\parallel$ from SRLS/NMR with fast GNM modes.

Fluctuation Distributions of the Slowest GNM Modes

Figure 6 displays the mobility profile of individual residues in the slowest GNM modes. The ordinates in Figure 6(a,b), respectively, show the normalized distribution of squared fluctuations driven by the first [Fig. 6(a)] and second [Fig. 6(b)] slowest modes, also called the first and second *global mode shapes*. The curves are directly found from the diagonal elements of the matrices $\mathbf{u}_1\mathbf{u}_1^T$ and $\mathbf{u}_2\mathbf{u}_2^T$ (eq 11) for AKeco (solid curve) and AKeco*AP_5A

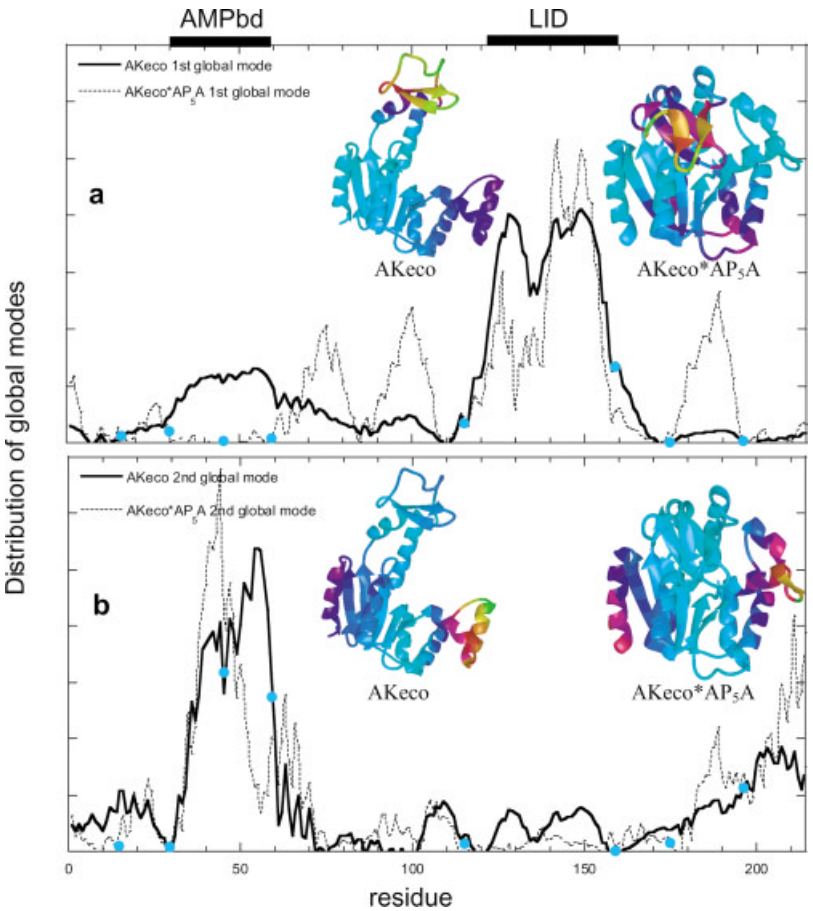

Fig. 6. First slowest global GNM mode shapes for AKeco (—) and AKeco*AP_5A (---) (**a**), and second slowest global GNM mode shapes for AKeco (—) and AKeco*AP_5A (---) (**b**). **Insets:** The ribbon diagrams of AKeco and AKeco*AP_5A color-coded cyan-blue-red-yellow-green in order of increasing mobility. The black boxes depict the LID and AMPbd domains. The blue dots denote residues associated by crystallographic studies[52] with hinges.

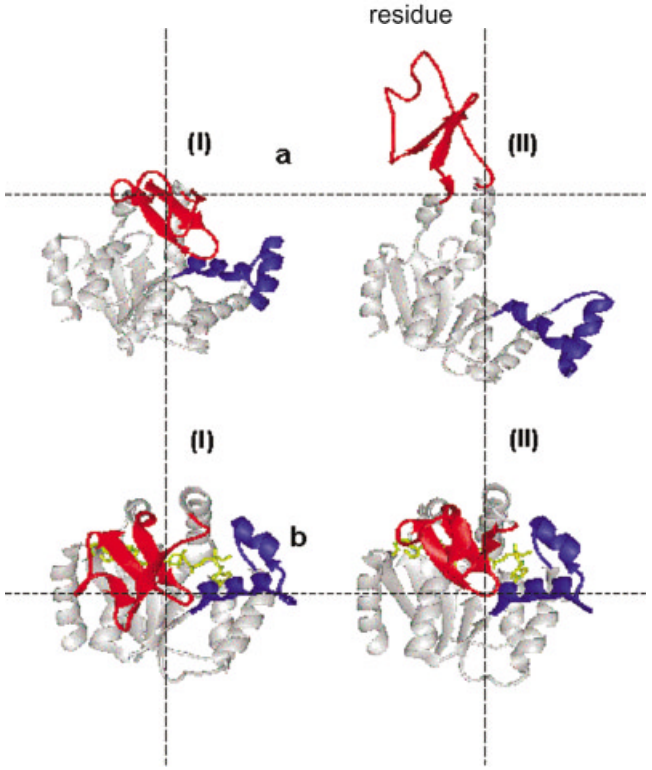

Fig. 7. Conformations I and II between which AKeco (**a**) and AKeco*AP_5A (**b**) fluctuate based on the first global mode according to ANM analysis. The LID and AMPbd domains are colored red and blue, respectively, and the inhibitor is colored yellow.

(dotted curve). The residue ranges of the AMPbd and LID domains are depicted by the black boxes on the upper abscissa [Fig. 6(a,b), top]. The insets in Figure 6(a,b) show the ribbon diagrams of AKeco and AKeco*AP_5A color-coded according to the magnitudes of the fluctuations associated with the first [Fig. 6(a)] and second [Fig. 6(b)] global modes. The color code is cyan-blue-red-yellow-green in the order of increasing mobility.

The slowest GNM mode of AKeco [solid curve in Fig. 6(a)] shows a broad peak in the region corresponding to LID residues, suggesting that this mode activates the catalysis-related movement of the LID domain. Interestingly, the solid curve in Figure 6(b) indicates that the second slowest GNM mode of AKeco activates the functional movement of the AMPbd domain. Thus, the domain motions of AMPbd and LID in the ligand-free enzyme are induced by different GNM modes. In the inhibitor-bound enzyme, the first global GNM mode induces notable mobility in the C-terminal segment of domain LID [dotted curve in Fig. 6(a)] and the second global GNM mode induces mobility in the N-terminal segment of domain AMPbd [dotted curve in Fig. 6(b)]. As pointed out previously,[14] and shown in Figure 4(d), NMR/SRLS analysis of in AKeco*AP_5A detected nanosecond motions in the α_2/α_3 loop of AMPbd and the C-terminal segment of domain LID. These apparently important dynamic elements associated with the catalytic transition state[14] can be now associated

with the second and first global GNM modes, respectively. We also note that a crystallographic study of a yeast adenylate kinase mutant bound to an ATP analogue pointed out independent motions of AMPbd and LID,[68] in agreement with the GNM results.

In addition to the activation of the LID domain, the slowest GNM mode of AKeco*AP_5A [dotted curve in Fig. 6(a)] induces enhanced (as compared to AKeco) mobility in the loops α_4/β_3 (residues Q74-G80) and α_5/β_4 (residues G100-P104), whereas in the ligand-free enzyme, the active site is flexible and the loops α_4/β_3 and α_5/β_4 are rigid. This is in agreement with the counterweight balancing of substrate binding hypothesis.[52] The second global GNM mode [Fig. 6(b)] activates the domain AMPbd and the C-terminal segment of the chain in both enzyme forms. There is a shift in mobility within AMPbd from the C-terminal part to the N-terminal part upon inhibitor binding. A crystallographic study of yeast adenylate kinase bound to AP_5A showed large B-factors within the C-terminal part of domain LID.[69] Finally, the chain segment A176-K195 is mobile in AKeco*AP_5A according to the first global GNM mode [dotted curve in Fig. 6(a)].

Hinge Centers and the Slowest GNM Modes

In general, hinge regions act as anchors about which domain (or loop) motions occur in opposite directions. In terms of GNM eigenvectors, hinge residues are located at the crossovers between the segments undergoing positive and negative fluctuations along the dominant principal/normal axes, and therefore form minima in the global mode shapes that refer to mean square fluctuations.

Based on the "fit-all" method applied to AKeco and AKeco*AP_5A eight hinges H1–H8, centered at residues T15, S30, L45, V59, L115, D159, T175, and V196, were identified by Muller et al.[52] It can be seen that residues T15, T175, and V196 coincide with (or closely neighbor) minima in the first global mode of AKeco, and residues T15, S30, L45, V59, T175, and V196 coincide with (or closely neighbor) minima in the first global mode of AKeco*AP_5A [Fig. 6(a)]. Residues T175 and V196 (S30 and D159) represent hinges in both enzyme forms according to the first (second) global GNM mode. Residues T15, S30, L115, D159, and T175 form minima in the second global mode of AKeco*AP_5A [dotted curve in Fig. 6(b)]. The first global GNM mode singles out the region around D110 as a hinge element for the flexing of the LID domain in both enzyme forms [Fig. 6(a)]. Hinges are typically associated with high order parameters. Seven out of the eight hinges of AKeco, the exception being hinge H7 (T175), feature high $S^2_{i\,GNM}$values [Fig. 4(a), solid curve]. High SRLS $(S^2_0)^2$ values were observed for five out of six (data are not available for residues S30 and D159) hinge residues in AKeco*AP_5A and AKeco. Order parameters are high for many residues. On the other hand, minima in the GNM global mode shapes single out hinges with high discrimination.

Mechanism/Biological Relevance of the Slowest Collective Modes Predicted by ANM

Figure 7 illustrates the most probable deformations, or global reconfigurations, obtained with ANM[23] for AKeco [Fig. 7(a)] and AKeco*AP_5A [Fig. 7(b)]. The ribbon diagrams I and II represent the two alternative (fluctuating) conformations driven by the slowest ANM mode using the PDB structures of the two enzyme forms[51,52] as starting conformations. For visual clarity, the LID (AMPbd) domain is colored red (blue), the inhibitor is colored yellow, and the fluctuations are amplified by a factor of 2.

Figure 7(a) indicates that the first global mode of the ligand-free enzyme drives a large-scale reconfiguration of the LID domain, which fluctuates between the "closed" (I) and "open" (II) forms. This tendency of LID to close over AMPbd, while the latter moves closer to LID, reflects the pre-disposition of the free enzyme to assume its inhibitor-bound form. This is consistent with crystallographic,[54] optical,[53] high temperature MD[70] studies, and a recent elastic normal mode analysis.[71]

Figure 7(b) and the dotted curve in Figure 6(a) indicate that the LID domain exhibits some mobility also in the inhibitor-bound enzyme. However, this motion is significantly more limited than that in AKeco, affecting the short solvent-exposed strands β_7 and β_8 and the connecting loop D147-G150 [Fig. 1(b)], while leaving the remaining portions of the LID docked onto the CORE. Proximity of the strands $\beta_7$and β_8 to the ATP-binding site and the salt bridges R123-D159 and R156-D158 involved in ATP binding[51] suggest involvement of these structural elements in transition state dissociation.

For the ligand-free form, the dominant motions elucidated with GNM are likely to be associated with "capturing" the substrates and properly positioning them for phosphoryl transfer. For the inhibitor-bound form, the dominant motions are likely to be associated with movements that initiate the dissociation of the transition state. Transition state dissociation appears to start with the C-terminal LID segment "opening up" the active site. Binding studies of AKeco also suggest that the active site region is flexible.[72] An optical study pointed out that AMP binding may modify the ATP binding site.[73] These are among the conclusions reached in a recent NMR study of μs-ms conformational exchange processes in AKeco and AKeco*AP_5A.[74]

The contact model proposed by Zhang and Bruschweiler[65] suggests that the local contacts experienced by the amide protons and carbonyl oxygens are the major determinant of S^2 values. The MD-based iRED approach[20] yields similar results. The GNM is also based on contact topology, which further supports the importance of the distribution of contacts in the native state. We note, however, that the contact model is usually suitable for estimating the fast time-scale dynamics of globular proteins, as contributions from long-range domain motions are not included. AKeco is a typical example of an enzyme featuring mobile domains engaged in large amplitude motions, and such cooperative motions cannot be adequately represented by a model based on local contacts

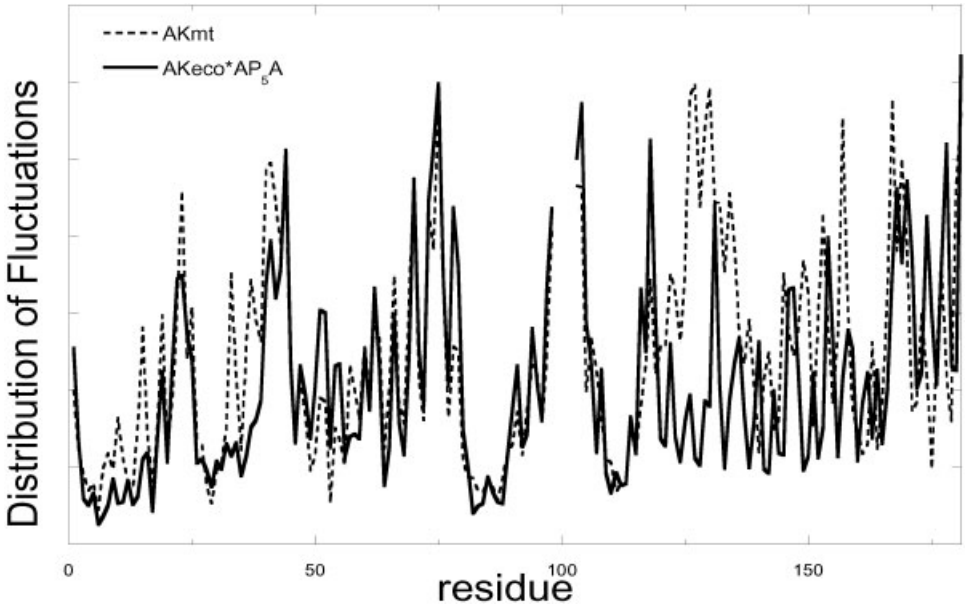

Fig. 8. Distribution of mean-square fluctuations determined with GNM for the AKmt solution structure[75] and the AKeco*AP_5A crystal structure[51] as a function of the AKmt sequence.

only. The GNM takes rigorous account of the long-range coupling of all native contacts, and permits us to identify the effect of a broad range of collective modes. The order parameters of the mobile domains important for function are indeed shown to be associated predominantly with slow (global) modes.

Validity of GNM Interpretation of NMR Data

GNM and SRLS are based on different models. GNM does not account for overall tumbling, but it yields both slow cooperative modes that activate entire domains and fast localized modes that relate to isolated N-H sites along the protein backbone. These are all "collective" modes in the sense that they depend on the coordinates of *all* the α-carbons and they are uniquely defined for the given topology of inter-residue contacts. SRLS accounts for the coupling of each N-H site to the overall tumbling of the protein. As shown by the results of the present study, GNM and SRLS can be compared meaningfully. Note that except for $\tau_0 = 2.5$ ns in eq 12, and the force constant γ in eq 10, GNM was used in this study as a predictive theory. Therefore, the agreement with the experiment-based SRLS analysis is quite rewarding.

The GNM calculations are based on the crystal structures of AKeco in the ligand-free and -bound forms. While the GNM satisfactorily reproduces the mobilities (B-factors) in the crystal forms, the fluctuations in the NMR solution structures could arguably be different, given that the proteins enjoy a higher flexibility in solution. On the other hand, previous applications of the GNM[21] to other proteins determined by both X-ray and NMR show that the fluctuation spectrum predicted by the GNM for the two groups of structures retain a large number of common features, because the fluctuations are essentially dominated by the topology of native contacts that are maintained in the different forms. Whether this feature also holds for adenylate kinase (AK) could be tested using the NMR structure of *Mycobacterium tuberculosis* adenylate kinase (AKmt) newly deposited in the PDB (PDB code: 1P4S).[75]

AKmt is 181 residues long while AKeco is 214 residues. The two sequences have 45% identity. There is a 4-residue insertion between α5 and β4 in AKmt and a 7-residue insertion between α8 and β5 in AKeco. AKeco LID domain is 27 residues longer than that of AKmt. The structure of AKmt matches the AKeco*AP_5A structure better than the apo enzyme AKeco. Superposition of the structures of AKmt and AKeco*AP_5A using CORE domain backbone atoms gives 2.8 Å rms deviation. This disagrees with optical studies that showed that ligand-free AK prevails *in solution* as a distribution of conformations,[53] peaked at the "open" conformation, rather than the closed form. An explanation for this discrepancy lies in the method of determining the NMR structure. The latter is based on NOE's that depend on $1/r^6$, where r denotes inter-proton distances on the order of 2.5–5.0 Å. Due to fast conformational averaging the experimentally measured NOE is a weighted average.[56] Because r is small and the NOE depends on it to the sixth power, the experimental NOE will be strongly biased toward short r-values associated with the "closed" form, leading to the latter structure instead of the weighted average structure.

Figure 8 compares the distribution of mean-square fluctuations predicted by the GNM for AKeco*AP_5A (crystal structure) and AKmt (solution structure). The agreement between the two sets of predicted results is remarkable, despite the sequence and structure differences between the two enzymes. This agreement lends support to the robustness of the GNM results, and suggests that many dynamic features elucidated in the present study are

conceivably generic, functional properties of adenylate kinases, conserved in different organisms. The unique potential of GNM to elucidate functional dynamics is thus highlighted.

CONCLUSIONS

N-H bond motion in adenylate kinase from *E. coli* is characterized by high NMR/SRLS order parameters and fast local motions ("ps regime" dynamics), or low NMR/SRLS order parameters and slow local motions ("ns regime" dynamics). It is shown herein that the former model correlates with fast stability-related localized GNM modes, and the latter with slow functional collective GNM modes. Catalysis-related motion of the domains LID and AMPbd in AKeco is activated by the first and second global GNM modes, respectively. The ANM analysis predicts functional dynamics configuring the active site in AKeco and bringing about transition state dissociation in AKeco*AP_5A. The rationalization of the mechanisms underlying the observed NMR relaxation behavior points out prospects for future GNM/ANM and NMR/SRLS studies aimed at relating structural dynamics to function.

ACKNOWLEDGMENTS

This work was supported in part by the NIGMS grant number 065805-01A1 (I.B.), the Israel Science Foundation (grant 520/99-16.1) and the Damadian Center for Magnetic Resonance research at Bar-Ilan University, Israel (E.M.). We acknowledge Dr. Y.E. Shapiro for carrying out the experiments of references 13, 14, and 56.

REFERENCES

1. Ishima R, Torchia DA. Protein dynamics from NMR. Nat Struct Biol 2000;7:740–743.
2. Kay LE. Protein dynamics from NMR. Nat Struct Biol 1998;5:513–517.
3. Palmer AG. NMR probes of molecular dynamics: Overview and comparison with other techniques. Annu Rev Biophys and Biomol Struct 2001;30:129–155.
4. Peng JW ,Wagner G. James TL ,Oppenheimer NJ, editor. Methods Enzymol. New York: Academic Press; 1994. p 563–595.
5. Lipari G, Szabo A. Model-free approach to the interpretation of nuclear magnetic resonance relaxation in macromolecules. 1. Theory and range of validity. J Am Chem Soc 1982;104:4546–4559.
6. Lipari G, Szabo A. Model-free approach to the interpretation of nuclear magnetic resonance relaxation in macromolecules. 2. Analysis of experimental results. J Am Chem Soc 1982;104:4559–4570.
7. Clore GM, Szabo A, Bax A, Kay LE, Driscoll PC, Gronenborn AM. Deviations from the simple two-parameter model-free approach to the interpretation of nitrogen-15 nuclear magnetic relaxation of proteins. J Am Chem Soc 1990;112:4989–4991.
8. Polimeno A ,Freed JH. a many-body stochastic approach to rotational motions in liquids. In: Prigogine I, Rice SA, editors. Advances in chemical physics. New York: John Wiley & Sons; 1993. p 89–210.
9. Polimeno A, Freed JH. Slow motional ESR in complex fluids: the slowly relaxing local structure model of solvent cage effects. J Phys Chem 1995;99:10995–11006.
10. Tugarinov V, Liang ZC, Shapiro YE, Freed JH, Meirovitch E. A structural mode-coupling approach to N-15 NMR relaxation in proteins. J Am Chem Soc 2001;123:3055–3063.
11. Meirovitch E, Shapiro YE, Tugarinov V, Liang Z, Freed JH. Mode-coupling analysis of ^{15}N CSA - ^{15}N-^{1}H dipolar cross-correlation in proteins. Rhombic potentials at the N-H bond. J Phys Chem 2003;107:9883–9897.
12. Meirovitch E, Shapiro YE, Tugarinov V, Liang Z, Freed JH. Mode-coupling SRLS versus mode-decoupled model-free N-H bond dynamics: mode-mixing and renormalization. J Phys Chem 2003; 107:9898–9904.
13. Tugarinov V, Shapiro YE, Liang Z, Freed JH, Meirovitch E. A novel view of domain flexibility in *E. coli* adenylate kinase based on structural mode-coupling 15N NMR relaxation. J Mol Biol 2002;315:155–170.
14. Shapiro YE, Kahana E, Tugarinov V, Liang ZC, Freed JH, Meirovitch E. Domain flexibility in ligand-free and inhibitor-bound *Escherichia coli* adenylate kinase based on a mode-coupling analysis of N-15 spin relaxation. Biochemistry 2002;41:6271–6281.
15. Brooks B, Karplus M. Harmoic dynamics of proteins:normal modes and fluctutuations in bovine pancreatic trypsin inhibitor. Proc Natl Acad Sci USA 1983;80:6571–6575.
16. Gibrat JF, Go N. Normal Mode Analysis of human lysozyme:study of the relative motion of the two domains and characterization of the harmonic motion. Proteins 1990;8:258–279.
17. Levitt M, Sander C, Stern PS. Protein normal-mode dynamics: trypsin inhibitor, crambin,ribonuclease and lysozyme. J Mol Biol 1985;181:423–447.
18. Amedei A, Linssen AB, Berendsen HJ. Essential dynamics of proteins. Proteins 1993;17:412–425.
19. Pfeiffer S, Fushman D, Cowburn D. Simulated and NMR-derived backbone dynamics of a protein with significant flexibility: a comparison of spectral densities for the betaARK1 PH domain. J Am Chem Soc 2001;123:3021–3036.
20. Prompers JJ, Bruschweiler R. Reorientational eigenmode dynamics: a combined MD/NMR relaxation analysis method for flexible parts in globular proteins. J Am Chem Soc 2001;123:7305–7313.
21. Bahar I, Atilgan AR, Erman B. Direct evaluation of thermal fluctuations in proteins using a single-parameter harmonic potential. Fold Des 1997;2:173–181.
22. Haliloglu T, Bahar I, Erman B. Gaussian dynamics of folded proteins. Phys Rev Lett 1997;79:3090–3093.
23. Atilgan AR, Durell SR, Jernigan RL, Demirel MC, Keskin O, Bahar I. Anisotropy of fluctuation dynamics of proteins with an elastic network model. Biophys J 2001;80:505–515.
24. Tirion MM. Large amplitude elastic motions in proteins from a single-parameter, atomic analysis. Phys Rev Lett 1996;77:1905–1908.
25. Bahar I. Dynamics of proteins and biomolecular complexes: Inferring functional motions from structure. Rev Chem Eng 1999;15:319–347.
26. Bahar I, Jernigan RL. Cooperative fluctuations and subunit communication in tryptophan synthase. Biochemistry 1999;38: 3478–3490.
27. Bahar I, Erman B, Jernigan RL, Atilgan AR, Covell DG. Collective motions in HIV-1 reverse transcriptase: examination of flexibility and enzyme function. J Mol Biol 1999;285:1023–1037.
28. Elezgaray J, Sanejouand YH. Modeling large-scale dynamics of proteins. Biopolymers 1998;46:493–501.
29. Hinsen K, Thomas A, Field MJ. Analysis of domain motions in large proteins. Proteins 1999;34:369–382.
30. Hinsen K, Thomas A, Field MJ. A simplified force field for describing vibrational protein dynamics over the whole frequency range. J Chem Phys 1999;111:10766–10769.
31. Doruker P, Atilgan AR, Bahar I. Dynamics of proteins predicted by molecular dynamics simulations and analytical approaches: application to alpha- amylase inhibitor. Proteins 2000;40:512–524.
32. Tama F, Gadea FX, Marques O, Sanejouand YH. Building-block approach for determining low-frequency normal modes of macromolecules. Proteins 2000;41:1–7.
33. Doruker P, Jernigan RL, Bahar I. Dynamics of large proteins through hierarchical levels of coarse-grained structures. J Comput Chem 2002;23:119–127.
34. Keskin O, Bahar I, Flatow D, Covell DG, Jernigan RL. Molecular mechanisms of chaperonin GroEL-GroES function. Biochemistry 2002;41:491–501.
35. Keskin O, Ji X, Blaszcyk J, Covell DG. Molecular motions and conformational changes of HPPK. Proteins 2002;49:191–205.
36. Keskin O, Durell SR, Bahar I, Jernigan RL, Covell DG. Relating molecular flexibility to function: a case study of tubulin. Biophys J 2002;663–680.
37. Ming D, Kong Y, Wakil SJ, Brink J, Ma J. Domain movements in

human fatty acid synthase by quantized elastic deformational model. Proc Natl Acad Sci USA 2002;99:7895–7899.
38. Ming D, Kong Y, Lambert MA, Huang Z, Ma J. How to describe protein motion without amino acid sequence and atomic coordinates. Proc Natl Acad Sci USA 2002;99:8620–8625.
39. Delarue M, Sanejouand YH. Simplified normal mode analysis of conformational transitions in DNA- dependent polymerases: the elastic network model. J Mol Biol 2002;320:1011–1024.
40. Tama F, Brooks CL, III. The mechanism and pathway of pH induced swelling in cowpea chlorotic mottle virus. J Mol Biol 2002;318:733–747.
41. Temiz NA, Bahar I. Inhibitor binding alters the directions of domain motions in HIV-1 reverse transcriptase. Proteins 2002;49: 61–70.
42. Kurkcuoglu O, Jernigan RL, Doruker P. Mixed levels of coarse-graining of large proteins using elastic network model succeeds in extracting the slowest motions. Polymer 2004;45:649–657.
43. Wang Y, Rader AJ, Bahar I, Jernigan RL. Global ribosome motions revealed with elastic network model. J Struct Biol 2004; doi:10.1016/j.jsb.2004. Forthcoming.
44. Xu CY, Tobi D, Bahar I. Allosteric changes in protein structure computed by a simple mechanical model: Hemoglobin T ↔ R2 transition. J Mol Biol 2003;333:153–168.
45. Zheng WJ, Doniach S. A comparative study of motor-protein motions by using a simple elastic-network model. Proc Natl Acad Sci USA 2003;100:13253–13258.
46. Bennett WS, Huber R. Structural and functional aspects of domain motions in proteins. CRC Crit Rev Biochem 1984;15:291–384.
47. Noda L. adenylate kinase. In: Boyer PD, editor. The Enzymes. New York: Academic Press; 1973. p 279–305.
48. Berry MB, Meador B, Bilderback T, Liang P, Glaser M, Phillips GN, Jr. The closed conformation of a highly flexible protein: the structure of *E. coli* adenylate kinase with bound AMP and AMPPNP. Proteins 1994;19:183–198.
49. Gerstein M, Lesk AM, Chothia C. Structural mechanisms for domain movements in proteins. Biochemistry 1994;33:6739–6749.
50. Muller-Dieckmann HJ, Schulz GE. Substrate specificity and assembly of the catalytic center derived from two structures of ligated uridylate kinase. J Mol Biol 1995;246:522–530.
51. Muller CW, Schulz GE. Structure of the complex between adenylate kinase from Escherichia coli and the inhibitor Ap5A refined at 1.9 A resolution. A model for a catalytic transition state. J Mol Biol 1992;224:159–177.
52. Muller CW, Schlauderer GJ, Reinstein J, Schulz GE. Adenylate kinase motions during catalysis: an energetic counterweight balancing substrate binding. Structure 1996;4:147–156.
53. Sinev MA, Sineva EV, Ittah V, Haas E. Domain closure in adenylate kinase. Biochemistry 1996;35:6425–6437.
54. Vonrhein C, Schlauderer GJ, Schulz GE. Movie of the structural changes during a catalytic cycle of nucleoside monophosphate kinases. Structure 1995;3:483–490.
55. Richard JP, Frey PA. Stereochemical course of thiophosphoryl group transfer catalyzed by adenylate kinase. J Am Chem Soc 1978;100:7757–7758.
56. Shapiro YE, Sinev MA, Sineva EV, Tugarinov V, Meirovitch E. Backbone dynamics of escherichia coli adenylate kinase at the extreme stages of the catalytic cycle studied by (15)N NMR relaxation. Biochemistry 2000;39:6634–6644.
57. Freed JH. Spin labeling:theory and applications. New York: Academic Press; 1976. 53 p.
58. Freed JH, Nayeem A, Rananavare SB. Luckhurst GR, Veracini CA, editor. The molecular dynamics of liquid crystals. Boston: Kluwer Academic Publishers; 1994. p 271–312.
59. Abragam A. Principles of nuclear magnetism. London: Oxford University Press; 1961.
60. Miyazawa S, Jernigan RL. Residue-residue potentials with a favorable contact pair term and an unfavorable high packing density term, for simulation and threading. J Mol Biol 1996;256: 623–644.
61. Haliloglu T, Bahar I. Structure-based analysis of protein dynamics: Comparison of theoretical results for hen lysozyme with X-ray diffraction and NMR relaxation data. Proteins 1999;37:654–667.
62. Bahar I, Erman B, Monnerie L. Kinematics of polymer-chains with freely rotating bonds in a restrictive environment. 1. Theory. Macromolecules 1992;25:6309–6314.
63. Bahar I, Erman B, Monerie L. Effect of molecular-structure on local chain dynamics: analytical approaches and computational methods. Adv Polym Sci 1994;116:145–206.
64. Go M, Go N. Fluctuations of an alpha-helix. Biopolymers 1976;15: 1119–1127.
65. Zhang FL, Bruschweiler R. Contact model for the prediction of NMR N-H order parameters in globular proteins. J Am Chem Soc 2002;124:12654–12655.
66. Kumar S, Sham YY, Tsai CJ, Nussinov R. Protein folding and function: the N-terminal fragment in adenylate kinase. Biophys J 2001;80:2439–2454.
67. Bahar I, Wallqvist A, Covell DG, Jernigan RL. Correlation between native-state hydrogen exchange and cooperative residue fluctuations from a simple model. Biochemistry 1998;37:1067–1075.
68. Abele U, Schulz GE. High-resolution structures of adenylate kinase from yeast ligated with inhibitor Ap(5)A, showing the pathway of phosphoryl transfer. Protein Sci 1995;4:1262–1271.
69. Schlauderer GJ, Proba K, Schulz GE. Structure of a mutant adenylate kinase ligated with an ATP-analogue showing domain closure over ATP. J Mol Biol 1996;256:223–227.
70. Elamrani S, Berry MB, Phillips GN, McCammon JA. Study of global motions in proteins by weighted masses molecular dynamics: adenylate kinase as a test case. Proteins 1996;25:79–88.
71. Tama F, Wriggers W, Brooks CL. Exploring global distortions of biological macromolecules and assemblies from low-resolution structural information and elastic network theory. J Mol Biol 2002;321:297–305.
72. Zhang HJ, Sheng XR, Pan XM, Zhou JM. Activation of adenylate kinase by denaturants is due to the increasing conformational flexibility at its active sites. Biochem Biophys Res Commun 1997;238:382–386.
73. Sinev MA, Sineva EV, Ittah V, Haas E. Towards a mechanism of AMP-substrate inhibition in adenylate kinase from *Escherichia coli*. FEBS Lett 1996;397:273–276.
74. Shapiro YE, Meirovitch E. Catalysis-related conformational exchange in *E. coli* adenylate kinase studied with ^{15}N NMR relaxation dispersion spectroscopy. J Phys Chem 2004; Forthcoming.
75. Miron S, Munier-Lehmann H, Craescu CT. Structural and dynamic studies on ligand-free adenylate kinase from Mycobacterium tuberculosis revealed a closed conformation that can be related to the reduced catalytic activity. Biochemistry 2004;43:67–77.
76. Kraulis PJ. *MOLSCRIPT*: a program to produce both detailed and schematic plots of protein structures. J Appl Crystallogr 1991;24: 946–950.